Supporting Information

A Broadband Near-Infrared Emission Na$_3$Al$_2$(PO$_4$)$_2$F$_3$: Cr^{3+} Phosphor

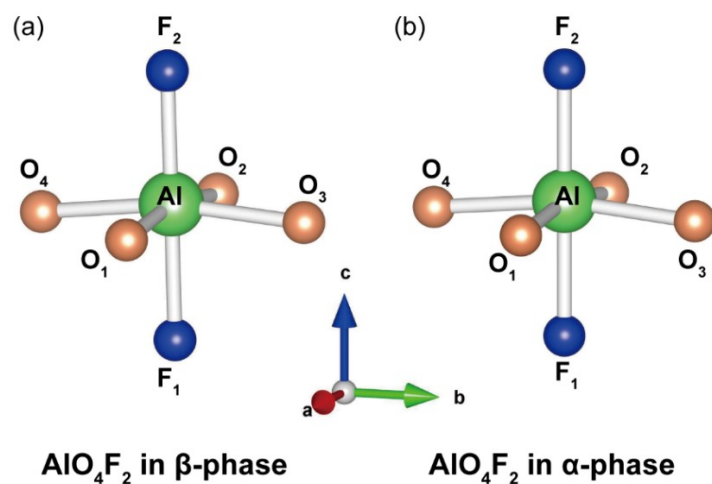## Exhibiting Zero Photoluminescence Quenching at 398 K

Huijie Wu [abc], Sisi Liang [*bc], Weixiong You [a], Le Liu [bc], Yongwei Guo [bc], Shujian Wang [bc], Liping Song [bc], Zihao Wang [bc] and Haomiao Zhu [*bc]
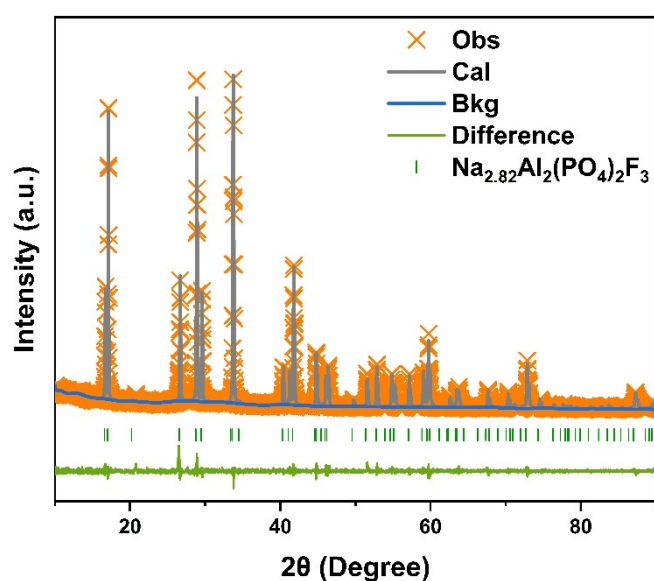
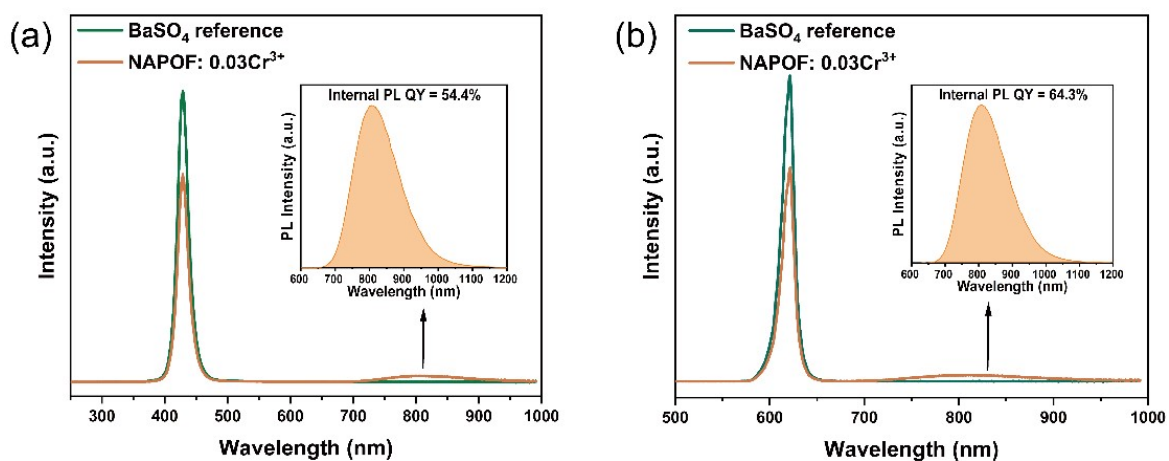**Figure S1** The Rietveld refinement on NAPOF: 0.03Cr^{3+} sample (α-phase).
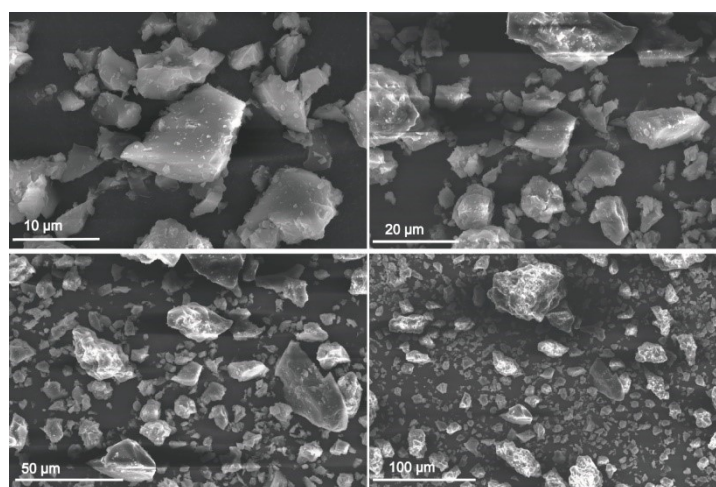
Figure S2 SEM images of NAPOF: 0.03Cr^{3+}.

Figure S3 Coordination of AlO_4F_2 in (a) β-phase and (b) α-phase of NAPOF.

bond length and bond angle data for AlO_4F_2 in β-phase and α-phase are provided in Table S4 and Table S5.

Figure S4 The measured spectra for calculating PL QY of the NAPOF: $0.03Cr^{3+}$ phosphor under (a) 420 nm and (b) 620 nm excitation, respectively.

Due to the limitation of the measurement, up to 990 nm, the results are smaller than the actual values. The spectrum before 990 nm accounted for 97% of the total. The value of PL QYs are obtained by adding up the two parts (650-990 nm for 97% and 990-1150 nm for 3%).
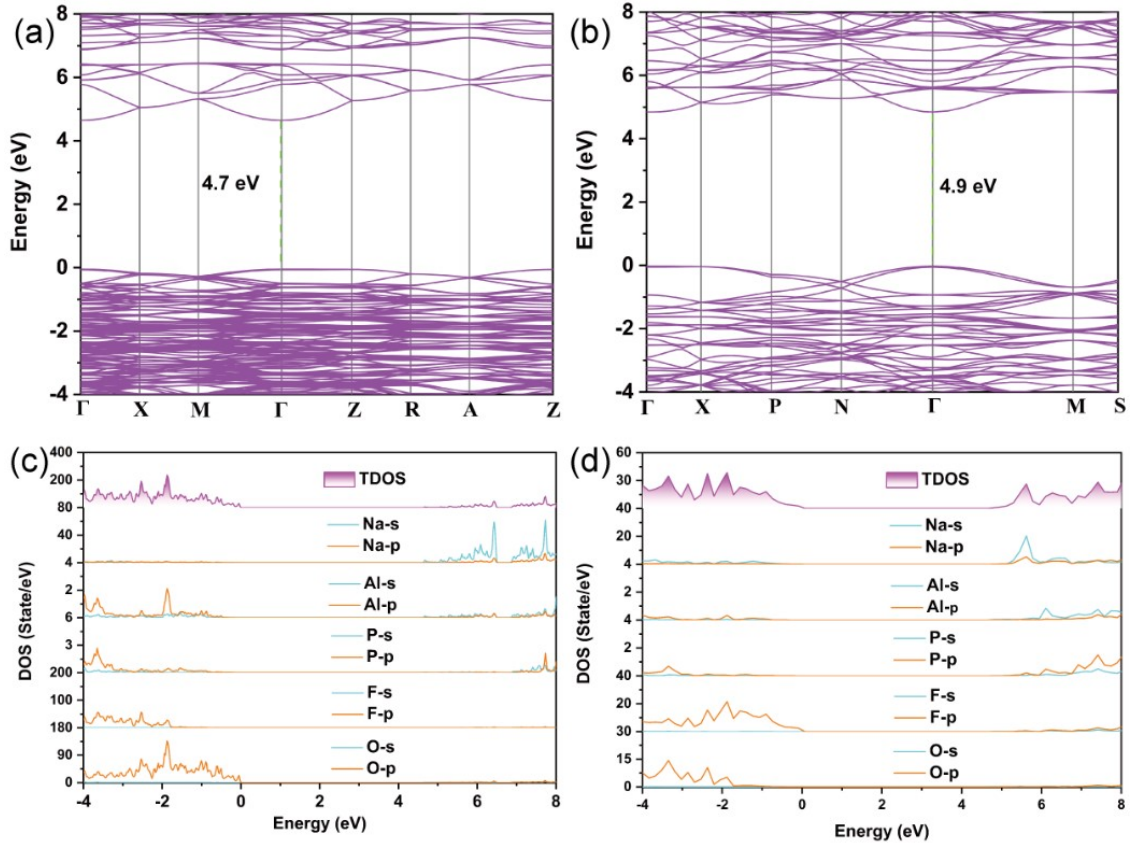
**Figure S5** The calculated band structures of (a) β-phase and (b) α-phase. The DOS of the orbitals of (c) β-phase and (d) α-phase.

Calculation Method: First-principles calculations are performed by vienna ab initio simulation package (VASP)[1, 2]. The generalized gradient approximation (GGA) of Perdew-Burke-Ernzerhof (PBE) is used to describe the exchange-correlation function[3]. The cut-off energy for the plane wave basis is set to 400 eV and a 2×2×2 Monkhorst-pack mesh is employed. All the structures are fully relaxed (atomic position) up to 10^{-4} eV/Å force minimization and max force of 0.01 eV/ Å. Considering the existence of different Na^+ positions in the system, we obtain an approximate model structure through ab–initio molecular dynamics (AIMD) for DFT calculation. DFT calculations are conducted without any symmetry constraints, thereby allowing Na atoms to relax into their most stable positions. The canonical (NVT) ensemble with the Nosé thermostat is used to conduct the molecular dynamics simulations and then scale to the appropriate temperature over 3000 time steps (2 ps).
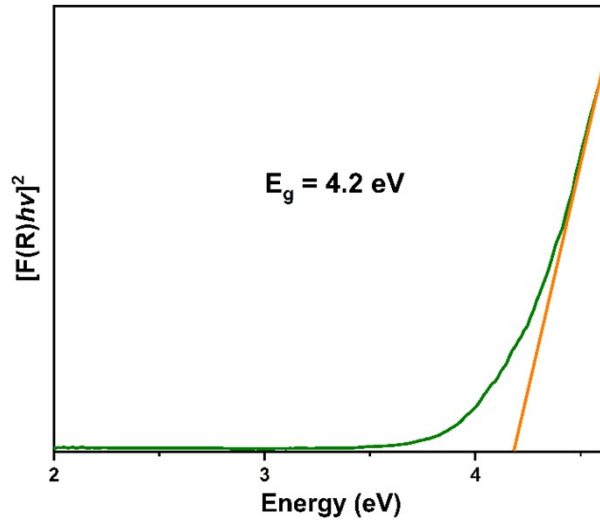
Figure S6 The relationship between the absorption coefficient and the photon energy for NAPOF.

On the basis of the Kubelka−Munk function, the optical band gap of the NAPOF host can be evaluated:[4]

$$F(R) = \frac{(1-R)^2}{2R} \tag{S1}$$

$$[F(R)hv]^{\frac{1}{n}} = A(hv - E_g) \tag{S2}$$

where F(R), R, hv, A, and Eg refer to the absorption, reflectance, photon energy, absorption constant, and optical band gap, respectively. The n values are 1/2 and 2 for the direct transition and indirect transition, respectively. The electronic band structure of NAPOF assign to a direct transition, so n = 1/2. The calculation result is shown in Figure S5 and the value of E_g is about 4.2 eV. The value is slightly lower than the value calculated by DFT (4.7 eV). The possible cause of this result is that the transparent light wavelength region of the crystal is wider than that of the powder.[5,6] The similar results are found in $NaScGe_2O_6$: Cr^{3+} and $KAlP_2O_7$: Cr^{3+} phosphors reported.[7,8]
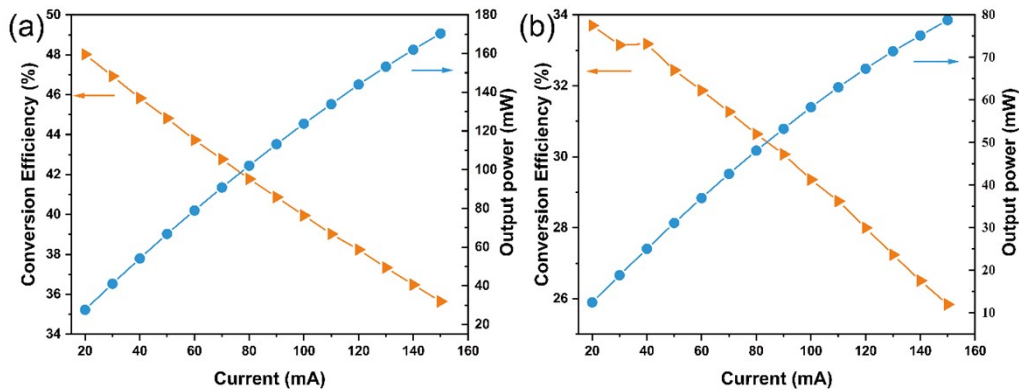
Figure S7 The output power and photoelectric efficiency with a drive current with 110 mA with (a) 420 nm and (b) 620 nm LED chips.

Table S1 Rietveld Refinement data and crystallographic data of NAPOF: $0.03Cr^{3+}$.

Phase	β	α
Space group	P42/mbc	I4mmm
Symmetry	Tetragonal	Tetragonal
a =b (Å)	12.400(1)	6.197(4)
C (Å)	10.410(1)	10.406(7)
α = β = γ (°)	90	90
Volume (Å^3)	1600.678	399.693
wR	9.7	8.6
GOF	1.6	1.2

Final refinement for β-phase: RF = 4.0% on 350 reflections. wR = 9.7% on 4001 observations in the histogram. Other residuals: R = 7.1%, R-bkg = 7.0%, wR-bkg = 9.7% wRmin = 6.0%, GOF = 1.6. Final refinement for α-phase: RF = 7.4% on 64 reflections. wR = 8.6% on 4001 observations in the histogram. Other residuals: R = 6.7%, R-bkg = 7.2%, wR-bkg = 8.6% wRmin = 7.1%, GOF = 1.2.

The observed large difference in the Rietveld profile could potentially be attributed to the following factors:

1. Different samples with identical structures are documented in Inorganic Crystal Structure Database (ICSD), such as $Na_{3.296}Al_2(PO_4)_2F_3$, $Na_{3.12}Al_2(PO_4)_2F_3$, and $Na_{2.82}Al_2(PO_4)_2F_3$ exhibiting slight variations in their diffraction patterns.

2. The SEM images of the NAPOF: $0.03Cr^{3+}$ are supplemented in the Figure S2. As we can see, the particles show unregular shapes. In practical, the powders with spherical shape are desired for measuring XRD patterns for refinement. The unregular shape of our sample may alter the diffraction intensity distribution.

Table S2 Refined structure parameters of NAPOF: 0.03Cr^{3+} (β-phase).

atom	x	y	z	frac	site sym	mult	Uiso
Na1	0.37330	0.59610	0.00000	0.6300	m (z)	8	0.01203
Na2	0.13020	0.59840	0.00000	0.6660	m (z)	8	0.01064
Na3	0.13480	0.32880	0.00000	0.1860	m (z)	8	0.05826
Na4	0.34060	0.37610	0.00000	0.4340	m (z)	8	0.01077
Na5	0.39250	0.50550	0.00000	0.4440	m (z)	8	0.02280
Na6	0.10950	0.50750	0.00000	0.1020	m (z)	8	0.03800
Na7	0.25130	0.35790	0.00000	0.4740	m (z)	8	0.01836
Na8	0.34170	0.62640	0.00000	0.3600	m (z)	8	0.00823
Al1	0.00010	0.24890	0.17930	0.985	1	16	0.00570
Cr	0.00010	0.24890	0.17930	0.015	1	16	0.00570
P1	0.00000	0.00000	0.25000	1.000	-4 (z)	4	0.00557
P2	0.00000	0.50000	0.25000	1.000	222(z)	4	0.00557
P3	0.24807	0.74807	0.25000	1.000	2(xy)	8	0.00494
F1	0.00230	0.25480	0.00000	1.000	m(z)	8	0.00583
F2	-0.00330	0.24510	0.35450	1.000	1	16	0.00899
O1	0.10220	0.00230	0.34050	1.000	1	16	0.00798
O2	0.59560	0.00080	0.33690	1.000	1	16	0.00836
O3	0.25000	0.34880	0.33580	1.000	1	16	0.00887
O4	0.75640	0.34900	0.34150	1.000	1	16	0.00595

Table S3 Refined structure parameters of NAPOF: 0.03Cr^{3+} (α-phase).

atom	x	y	z	frac	site sym	mult	Uiso
Na1	0.28230	0.28230	0.00000	0.4960	mm2 (xy)	8	0.03800
Na2	0.50000	0.22600	0.00000	0.2080	mm2 (y)	8	0.11399
Al1	0.00000	0.00000	0.17930	0.9850	4mm(z)	4	0.00560
Cr	0.00000	0.00000	0.17930	0.0150	4mm(z)	4	0.00560
P1	0.00000	0.50000	0.25000	1.000	-4m (2z)	4	0.00464
O1	0.00000	0.30260	0.16185	1.000	m (x)	16	0.00999
F1	0.00000	0.00000	0.00000	1.000	4/mmm (z)	2	0.00760
F2	0.00000	0.00000	0.35430	1.000	4mm (z)	4	0.01229

Table S4 Bond length data for AlO_4F_2 (β-phase and α-phase).

Phase Bond	β-phase length (Å)	α-phase length (Å)
F_1-Al	1.8640(12)	1.8679(10)
F_2-Al	1.821(3)	1.8232(15)
O_1-Al	1.828(4)	1.8867(4)
O_2-Al	1.933(4)	1.8867(4)
O_3-Al	1.886(8)	1.8867(7)
O_4-Al	1.878(8)	1.8867(7)

Table S5 Bond angle data for AlO_4F_2 (β-phase and α-phase).

Phase Bond	β-phase angle (°)	α-phase angle (°)
F_1-Al-F_2	179.1(3)	180
F_1-Al-O_1	85.80(13)	84.47(8)
F_1-Al-O_2	82.76(14)	84.47(8)
F_1-Al-O_3	84.2(3)	84.47(8)
F_1-Al-O_4	84.4(3)	84.47(8)
F_2-Al-O_1	94.96(13)	95.53(8)
F_2-Al-O_2	96.48(15)	95.53(8)
F_2-Al-O_3	95.3(3)	95.53(8)
F_2-Al-O_4	96.1(3)	95.53(8)

Table S6 Comparison of the mechanism of zero-thermal quenching phosphors.

Phosphor	Mechanism	Ref.
NAPOF: Cr^{3+}	high structure rigidity	this
	wide band gap	work
$Na_3Sc_2(PO_4)_3$: Eu^{2+}	energy transfer leads to emission compensation	[9]
$Na_3Al_2Li_3F_{12}$: Cr^{3+}	high structure rigidity	[10]
$Y_3In_2Ga_3O_{12}$: Cr^{3+}	high structure rigidity	[11]
	wide band gap	
$LaAlO_3$: Mn^{4+}	energy transfer leads to emission compensation	[12]
$Zn_{0.85}Li_{0.15}Ga_2O_{4-\delta}$: Cr^{3+}	energy transfer leads to emission compensation	[13]

The rigid lattice structure and broad bandgap are the main reason to resist the thermal quenching, and we confirm the rigidity of NAPOF: Cr^{3+} by the discussion as follow:

1. The relatively small Huang-Rhys factor (S = 2.7) represents a medium strength electron-

phonon coupling (EPC) and small ΔR (which represents small Stokes shift). Notably, the value of ΔR is qualitative measure of the interaction between the absorbing metal ion and the vibrations of its surroundings, i.e., the interaction between the electrons and the vibrations of the optical centre under consideration.[14] The small ΔR implies a rigid structure.[15] Figure 5d depicts the mechanism.

2. The normalized PL spectra of NAPOF: $0.03Cr^{3+}$ at 298 – 473 K show a negligible shift of the peak emission wavelength (Figure 5b), indicating a slight expansion in the local crystal field environment surrounding Cr^{3+} ions.

3. NAPOF has the rigid three dimensional framework formed by PO_4 tetrahedral and $Al_2O_8F_3$ bioctahedra corner-connecting with each other. The $Al_2O_8F_3$ bioctahedra, which share one apex F atom. This shared vertex structure may enhance the rigidity of the octahedra, thus contributing to the phosphor's good PL thermal stability.

Furthermore, in Dorenbos' thermal ionization model, the excited electrons are ionized at high temperatures and directly transition to the conduction band without returning to the ground state. The relatively wide bandgap of host may be beneficial to avoid the occurrence of thermal ionization, e.g., K_2BaPO_4F: Eu^{2+} (6.2 eV, 100%@ 423K)[16], $Y_3In_2Ga_3O_{12}$: Cr^{3+} (5.0 eV, 100@ 423 K).[11]

There are some other mechanisms have been proposed to explain the zero thermal quenching property in previous literature. The energy transfer between defect and excited state may leads to emission compensation. In this mechanism, the excited electrons are trapped by the defect level. With the temperature rises, the electrons are de-trapped and thermal activated to the excited level, eventually transiting back to the ground state with radiation.[9, 12, 13] This mechanism is logical, but we cannot provide the exact evidence to confirm the contribution of the defects in NAPOF: Cr^{3+}. The mechanism of some zero thermal quenching phosphors were compared in Table S6.

Supplementary calculation

Table S7 $(FWHM)^2$ and $1/(2kT)$ at different temperatures

$(FWHM)^2$ (eV^2)	$1/(2kT)$ $(1/eV)$
0.08910	19.5
0.0925	18.0
0.0960	16.7
0.1019	15.6
0.1029	14.6
0.1075	13.7
0.1116	12.9
0.1135	12.1

In view of $\hbar\omega/kT \approx 10^{-3}$, the above equation can be approximated as[7]

$$FWHM^2 = 5.57 \times S \times (\hbar\omega)^2 \left(1 + \cfrac{1}{\hbar\omega/2kT} \right) \tag{S3}$$

The values of FWHM at different temperatures were subjected to a nonlinear curve fitting analysis, yielding the subsequent outcome.

$$FWHM^2 = 0.04642 + \cfrac{1}{\cfrac{1}{2kT}}$$

In this way, S and $\hbar\omega$ values are calculated to be 2.7 and 55.6 meV, respectively.

References

1. G. Kresse and J. Furthmuller, *Comput. Mater. Sci*, 1996, **6**, 15-50.
2. G. Kresse and D. Joubert, *Phys. Rev. B: Condens. Matter*, 1999, **59**, 1758-1775.
3. J. P. Perdew, K. Burke and M. Ernzerhof, *Phys. Rev. Lett.*, 1996, **77**, 3865-3868.
4. R. López and R. Gómez, *J. Sol-Gel Sci. Technol.*, 2012, **61**, 1-7.
5. J. Y. Xiang, J. W. Yang, N. J. Luo, J. Zhu, S. P. Huang and Y. Mao, *Results Phys.*, 2019, **13**.102258.
6. J. Zhu, W. D. Cheng, D. S. Wu, H. Zhang, Y. J. Gong and H. N. Tong, *J. Solid State Chem.*, 2006, **179**, 597-604.
7. X. F. Zhou, W. Y. Geng, J. Y. Li, Y. C. Wang, J. Y. Ding and Y. H. Wang, *Adv. Opt. Mater.*, 2020, **8**, 1902003.
8. H. S. Zhang, J. Y. Zhong, F. Du, L. Chen, X. L. Zhang, Z. F. Mu and W. R. Zhao, *ACS Appl. Mater. Interfaces*, 2022, **14**, 11663-11671.
9. Y. H. Kim, P. Arunkumar, B. Y. Kim, S. Unithrattil, E. Kim, S. H. Moon, J. Y. Hyun, K. H. Kim, D. Lee, J. S. Lee and W. B. Im, *Nat. Mater.*, 2017, **16**, 543-550.
10. D. C. Huang, S. S. Liang, D. J. Chen, J. Hu, K. Y. Xu and H. M. Zhu, *Chem. Eng. J.*, 2021, **426**, 131332.
11. C. J. Li and J. Y. Zhong, *Chem. Mater.*, 2022, **3**, 8418-8426.
12. S. Q. Fang, T. C. Lang, T. Han, J. Y. Wang, J. Y. Yang, S. X. Cao, L. L. Peng, B. T. Liu, A. N. Yakovlev and V. I. Korepanov, *Chem. Eng. J.*, 2020, **389**, 124297.
13. J. C. Lu, Q. Liu, X. H. Chen, K. Y. Li, W. Chen, Y. B. Feng, S. Liu, X. Qian, B. Wei and L. Zhang, *Ceram. Int.*, 2023, **49**, 19062-19071.
14. G. Blasse, B. Grabmaier, G. Blasse and B. Grabmaier, Luminescent Materials, 1994, 10-32.
15. G. Blasse, B. Grabmaier, G. Blasse and B. Grabmaier, Luminescent Materials, 1994, 33-70.
16. Z. Leng, D. Zhang, H. Bai, H. He, Q. Qing, J. Zhao and Z. Tang, *J. Mater. Chem. C*, 2021, **9**, 13722-13732.